DESY 21-078

The strong CP problem solved by itself due to long-distance vacuum effects

Y. Nakamura[a] and G. Schierholz[b]

[a] RIKEN Center for Computational Science,
Kobe, Hyogo 650-0047, Japan
[b] Deutsches Elektronen-Synchrotron DESY,
22603 Hamburg, Germany

Abstract

The vacuum of quantum chromodynamics has an incredibly rich structure at the nonperturbative level, which is intimately connected with the topology of gauge fields, and put to a stringent test by the strong CP problem. We investigate the long-distance properties of the theory in the presence of a topological θ term. This is done on the lattice, using the gradient flow to isolate the long-distance modes in the functional integral measure and tracing it over successive length scales. We find that the color fields produced by quarks and gluons are screened for vacuum angles $|\theta| > 0$, thus providing a natural solution of the strong CP problem.

1 Introduction

Quantum chromodynamics (QCD) decribes the strong interactions remarkably well, from the smallest distances probed so far to hadronic scales where quarks and gluons confine to hadrons. Yet it faces a problem. The theory allows for a CP-violating term S_θ in the action. In Euclidean space-time it reads

$$S_\theta = i\,\theta\,Q\,, \quad Q = \frac{1}{32\pi^2}\int d^4x\; F^a_{\mu\nu}\tilde{F}^a_{\mu\nu} \in \mathbb{Z}\,, \tag{1}$$

where Q is the topological charge, and θ is an arbitrary phase with values $-\pi < \theta \leqslant \pi$. A nonvanishing value of θ would result in an electric dipole moment d_n of the neutron. The current experimental upper limit is $|d_n| < 1.8 \times 10^{-13} e\,\mathrm{fm}$ [1], which suggests that θ is anomalously small. This feature is referred to as the strong CP problem, which is considered as one of the major unsolved problems in the elementary particles field.

It is known from the case of the massive Schwinger model [2] that a θ term may change the phase of the system. Callan, Dashen and Gross [3] have claimed that a similar phenomenon will occur in QCD. The statement is that the color fields produced by quarks and gluons will be screened by instantons for $|\theta| > 0$. 't Hooft [4] argued that at intermediate length scales the relevant degrees of freedom responsible for confinement are color-magnetic monopoles. This is realized by a partial gauge fixing [5], which leaves the maximal abelian subgroup U(1)×U(1) unbroken. Quarks and gluons have color-electric charges with respect to the U(1) subgroups. Ordinary confinement occurs when the monopoles condense in the vacuum, by analogy to superconductivity. This has first been verified on the lattice by Kronfeld *et al.* [6]. In the presence of a θ term the monopoles acquire a fractional color-electric charge, shown by Witten [7]. In this case the color(-electric) fields are expected to be screened by monopoles, driving the theory into a Higgs or Coulomb phase [4, 8] for $|\theta| > 0$. On the other hand, isolated instantons are found to consist of closed loops of monopoles carrying half-integer color-electric charge, with alternate sign for instanton and anti-instanton [9]. In the confining vacuum instantons and anti-instantons are supposed to overlap strongly, so that the monopoles can move freely from one (anti-)instanton to the other. A nonvanishing value of θ causes an imbalance of instantons and anti-instantons. This results in a net color-electric charge proportional to θ, in accordance with [7], which reconciles the different views.

Taken together, this strongly suggests that θ is restricted to zero in the confining phase of the theory, which would mean that the strong CP problem is solved by itself. A direct derivation of the phase structure of QCD for nonvanishing values of θ from first principles has remained elusive. Lattice gauge theory is the only available tool to address this problem. The difficulty is that a single gauge field covers the entire frequency spectrum of the theory, from short distance fluctuations to monopoles and instantons, while one is interested in the properties and evolution of the system at progressively larger length scales. This requires to isolate the long-distance modes in the functional integral measure and tracing it over successive scales in a controlled fashion.

The framework for dealing with physical problems involving different energy scales is the multi-scale renormalization group (RG) flow. It defines a universal overall renormalization scale (or cutoff) μ, with respect to which the force laws underlying the physical system change. Varying μ, the couplings and Green functions satisfy standard (although scheme dependent) RG equa-

tions. Exact RG schemes are very difficult to implement numerically. The gradient flow [10, 11] provides a powerful alternative for scale setting, with no need for costly ensemble matching. It is a particular realization of the coarse-graining step of momentum space RG transformations [12, 13, 14, 15], and as such can be used to study RG transformations directly.

In this Letter we investigate the long-distance properties of the theory in the presence of the θ term (1) using the gradient flow, and show that CP is naturally conserved in the confining phase.

2 The gradient flow

The gradient flow describes the evolution of fields and physical quantities as a function of flow time t. The flow of SU(3) gauge fields is defined by [11]

$$\partial_t B_\mu(t,x) = D_\nu G_{\mu\nu}(t,x)\,, \quad G_{\mu\nu} = \partial_\mu B_\nu - \partial_\nu B_\mu + [B_\mu, B_\nu]\,, \quad D_\mu \cdot = \partial_\mu \cdot + [B_\mu, \cdot]\,, \tag{2}$$

where $B_\mu(t,x) = B^a_\mu(t,x)\,T^a$, and $B_\mu(t=0,x) = A_\mu(x)$ is the original gauge field of QCD. It thus defines a sequence of gauge fields parameterized by t. The renormalization scale μ is set by the flow time, $\mu = 1/\sqrt{8t}$ for $t \gg 0$. Correlators of the flow fields are automatically renormalized [16]. The expectation value of the energy density

$$E(t,x) = \frac{1}{2}\,\mathrm{Tr}\,G_{\mu\nu}(t,x)\,G_{\mu\nu}(t,x) = \frac{1}{4}\,G^a_{\mu\nu}(t,x)\,G^a_{\mu\nu}(t,x) \tag{3}$$

defines a renormalized coupling

$$g^2_{GF}(\mu) = \frac{16\pi^2}{3}\,t^2\langle E(t)\rangle\big|_{t=1/8\mu^2} \tag{4}$$

at flow time t in the gradient flow scheme.

For a start we may restrict our investigations to the Yang-Mills theory. If the strong CP problem is resolved in the Yang-Mills theory, then it is expected that it is also resolved in QCD.

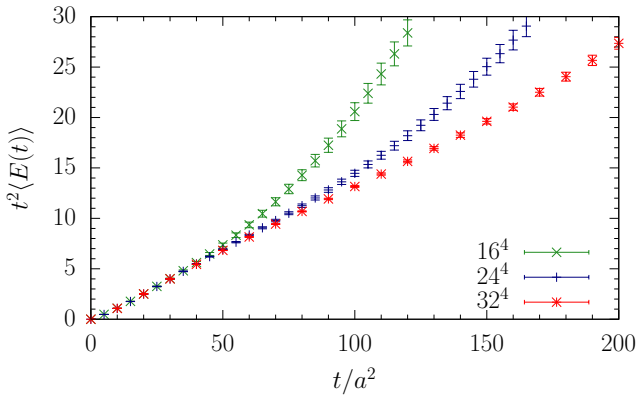

Figure 1: The dimensionless quantity $t^2\langle E(t)\rangle$ as a function of t/a^2 on the 16^4, 24^4 and 32^4 lattice.

We use the plaquette action [17]

$$S = \beta \sum_{x,\mu<\nu} \left(1 - \frac{1}{3} \mathrm{Re\,Tr}\, U_{\mu\nu}(x)\right). \tag{5}$$

to generate representative ensembles of fundamental gauge fields. For any such gauge field the flow equation (2) is integrated to the requested flow time t. We use a continuum-like version of the energy density $E(t,x)$ obtained from a symmetric (clover-like) definition of the field strength tensor $G_{\mu\nu}(t,x)$ [11]. The simulations are done for $\beta = 6/g^2 = 6.0$ on 16^4, 24^4 and 32^4 lattices. The lattice spacing at this value of β is $a = 0.082(2)$ fm, where we have taken $\sqrt{t_0} = 0.147(4)$ fm to set the scale [18, 19], with t_0 defined by $t_0^2\langle E(t_0)\rangle = 0.3$. Our current ensembles include 4000 configurations on the 16^4 lattice and 5000 configurations on the 24^4 and 32^4 lattices each. First results on the smaller lattices have been reported in [20].

We consider flow times up to $t/a^2 = 200$, but will limit the evaluation of physical quantities to $t/a^2 \leqslant 100$. In Fig. 1 we show the dimensionless quantity $t^2\langle E(t)\rangle$ on the 16^4, 24^4 and 32^4 lattice as a function of t/a^2. The data on the 32^4 lattice fall on a straight line up to $t/a^2 \approx 200$. The data on the smaller lattices show finite volume effects for $\tau \equiv \sqrt{8t} \gtrsim L$, where L is the length of the lattice, which is to be expected. Unlike $t^2\langle E(t)\rangle$, physical quantities ought to be independent of the RG scale. In the Yang-Mills theory the choice of observables that can be computed accurately is limited. Two such quantities are the topological susceptibility and the (re)normalized Polyakov loop susceptibility. The topological susceptibility is defined by

$$\chi_t = \frac{\langle Q^2\rangle - \langle Q\rangle^2}{V}, \tag{6}$$

where $V = L^4$. We define the (re)normalized Polyakov loop susceptibility by

$$\chi_P = \frac{\langle |P|^2\rangle - \langle |P|\rangle^2}{\langle |P|\rangle^2}, \tag{7}$$

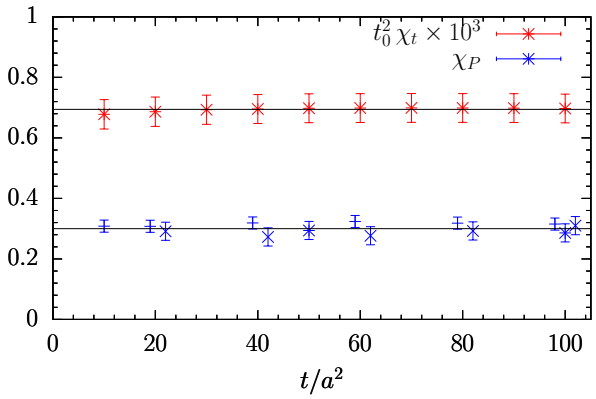

Figure 2: The topological susceptibility χ_t on the 32^4 lattice, and the Polyakov loop susceptibility χ_P on the 16^4 (+), 24^4 (×) and 32^4 (∗) lattice.

where

$$P = \frac{1}{V_3}\sum_{\vec{x}} P(\vec{x})\,, \quad P(\vec{x}) = \frac{1}{3}\,\mathrm{Tr}\prod_{x_0=0}^{L-a} U_0(x_0,\vec{x}) \tag{8}$$

with $U_0(x_0,\vec{x})$ being the (complex valued) link matrix in time direction and V_3 the spatial volume, $V_3 = L^3$. Note that $\langle|P|^2\rangle$ denotes the Polyakov loop correlator

$$\langle|P|^2\rangle = \frac{1}{V_3}\sum_{\vec{x}}\langle P(0)\,P^\dagger(\vec{x})\rangle\,. \tag{9}$$

In Fig. 2 we show χ_t and χ_P as a function of flow time for $t/a^2 = 10$ to 100. Both quantities are independent of t within the errorbars, as expected. A linear fit to the topological susceptibility gives $\sqrt{t_0}\chi_t^{1/4} = 0.162(3)$. This result agrees precisely with the value reported in [21], $\sqrt{t_0}\chi_t^{1/4} = 0.161(4)$. A linear fit to the Polyakov loop susceptibility gives $\chi_P = 0.289(7)$. For comparison, a 2D Gaussian distribution of real and imaginary P yields $\chi_P = 4/\pi - 1 = 0.273$, which is close to the lattice result. Similarly, defining χ_Q by substituting P with Q in eq. (7), we derive $\chi_Q = \pi/2 - 1 = 0.571$, assuming a Gaussian distribution of the topological charge Q. The lattice result is $\chi_Q = 0.505(33)$.

3 Running coupling and linear confinement

The gradient flow running coupling $\alpha_{GF}(\mu) = g^2_{GF}(\mu)/4\pi$, introduced in (4), plays a key role in our investigations. In Fig. 3 we show α_{GF}/π on the 32^4 lattice as a function of $t/a^2 = 1/8\,a^2\mu^2$. The stunning result is that α_{GF} is a clearly linear function of $1/\mu^2$ in the nonperturbative regime down to $\mu \approx 100$ MeV and below. This results in the gradient flow beta function

$$\frac{\partial\,\alpha_{GF}(\mu)}{\partial\,\ln\,\mu} \equiv \beta_{GF}(\alpha_{GF}) \underset{\mu \ll 1\,\mathrm{GeV}}{=} -2\,\alpha_{GF}(\mu)\,. \tag{10}$$

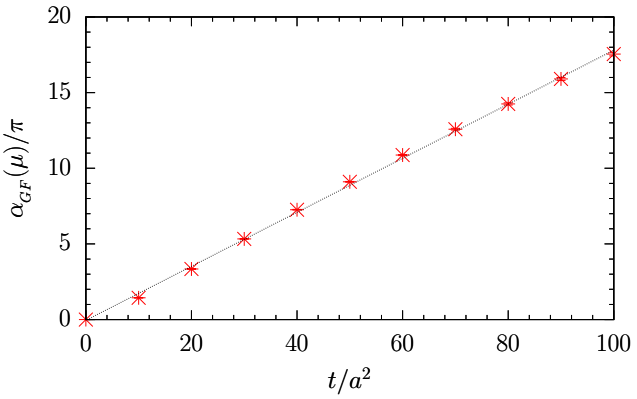

Figure 3: The gradient flow coupling $\alpha_{GF}(\mu)/\pi$ on the 32^4 lattice as a function of t/a^2, together with a linear fit.

For arbitrary values of μ the RG equation (10) has the implicit solution

$$\frac{\Lambda_{GF}}{\mu} = (4\pi b_0 \alpha_{GF})^{-\frac{b_1}{2b_0^2}} \exp\left\{ -\frac{1}{8\pi b_0 \alpha_{GF}} - \int_0^{\alpha_{GF}} d\alpha \, \frac{1}{\beta_{GF}(\alpha)} + \frac{1}{8\pi b_0 \alpha^2} + \frac{b_1}{2b_0^2 \alpha} \right\}, \tag{11}$$

which leads to

$$\alpha_{GF}(\mu) \underset{\mu \ll 1\,\mathrm{GeV}}{=} \frac{\Lambda_{GF}^2}{\mu^2}. \tag{12}$$

A fit of (12) to the lattice data shown in Fig. 3 gives $\sqrt{t_0}\,\Lambda_{GF} = 0.475(16)$.

To make contact with phenomenology, it is desirable to transform the gradient flow coupling α_{GF} to a common scheme. A preferred scheme in the Yang-Mills theory is the V scheme [22]. In this scheme

$$\frac{\Lambda_V}{\mu} = (4\pi b_0 \alpha_V)^{-\frac{b_1}{2b_0^2}} \exp\left\{ -\frac{1}{8\pi b_0 \alpha_V} - \int_0^{\alpha_V} d\alpha \, \frac{1}{\beta_V(\alpha)} + \frac{1}{8\pi b_0 \alpha^2} + \frac{b_1}{2b_0^2 \alpha} \right\}. \tag{13}$$

If we divide eq. (11) by eq. (13) we arrive at the relation

$$\frac{\Lambda_{GF}}{\Lambda_V} = \exp\left\{ -\int_0^{\alpha_{GF}} d\alpha \, \frac{1}{\beta_{GF}(\alpha)} + \int_0^{\alpha_V} d\alpha \, \frac{1}{\beta_V(\alpha)} \right\}. \tag{14}$$

Using (10) and (12), we can solve eq. (14) for $\beta_V(\alpha_V)$ and $\alpha_V(\mu)$ in the nonperturbative regime. The result is

$$\beta_V(\alpha_V) \underset{\mu \ll 1\,\mathrm{GeV}}{=} -2\,\alpha_V(\mu), \quad \alpha_V(\mu) \underset{\mu \ll 1\,\mathrm{GeV}}{=} \frac{\Lambda_V^2}{\mu^2}. \tag{15}$$

From the literature we know $\Lambda_V/\Lambda_{\overline{MS}} = 1.600$ [22] and $\Lambda_{\overline{MS}}/\Lambda_{GF} = 0.534$ [11]. This leads to $\sqrt{t_0}\,\Lambda_V = 0.406(14)$ and $\sqrt{t_0}\,\Lambda_{\overline{MS}} = 0.217(7)$. The latter number is in excellent agreement with the outcome of a recent dedicated lattice calculation [23], $\sqrt{t_0}\,\Lambda_{\overline{MS}} = 0.220(3)$.

The linear growth of $\alpha_V(\mu)$ with $1/\mu^2$, which is commonly dubbed infrared slavery, effectively describes many low-energy phenomena of the theory. So, for example, the static quark-antiquark potential, which can be described by the exchange of a single dressed gluon, $V(q) = -\frac{4}{3}\,\alpha_V(q)/q^2$. A popular example is the Richardson potential [24], which reproduces the spectroscopy of heavy quark systems, like charmonium and bottomonium, very well. Upon performing the Fourier transformation of $V(q)$ to configuration space, we obtain

$$V(r) = -\frac{1}{(2\pi)^3} \int d^3\mathbf{q} \; e^{i\,\mathbf{qr}} \; \frac{4}{3} \, \frac{\alpha_V(q)}{\mathbf{q}^2 + i0} \underset{r \gg 1/\Lambda_V}{=} \sigma\, r, \tag{16}$$

where σ, the string tension, is given by $\sigma = \frac{2}{3}\,\Lambda_V^2$. The result is $\sqrt{t_0\,\sigma} = 0.331(11)$. Converted to physical units, we obtain $\sqrt{\sigma} = 445(19)$ MeV, which is exactly what one expects from Regge phenomenology.

4 Phase structure in the presence of the θ term

With increasing flow time the initial gauge field ensemble splits into effectively disconnected topological sectors of charge Q. That is known to us already from 'cooling' lattice gauge field

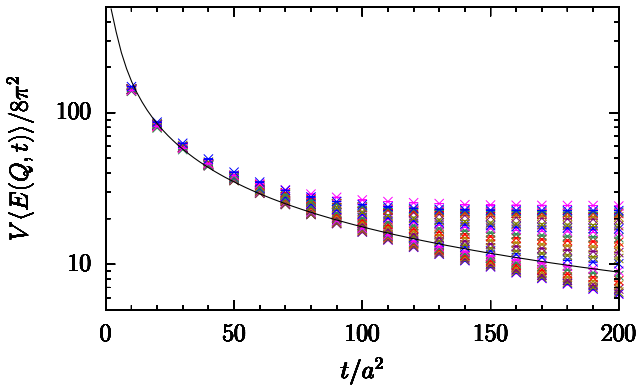

Figure 4: The action $V\langle E(Q,t)\rangle/8\pi^2$ of the different topological sectors as a function of t/a^2 on the 32^4 lattice for charges ranging from $Q = 0$ (bottom) to $|Q| = 22$ (top). The solid line represents the ensemble average.

configurations [25, 26]. We distinguish the topological sectors by the affix Q. The first quantity we look at is the energy density $\langle E(Q,t)\rangle$ in form of the 'action' $S_Q = V\langle E(Q,t)\rangle/8\pi^2$, which we normalized to give $S_Q = |Q|$ for a semi-classical multi-instanton configuration of charge Q. In Fig. 4 we show S_Q on the 32^4 lattice as a function of t/a^2. From this we see that $V\langle E(Q,t)\rangle/8\pi^2 \simeq |Q|$ at large flow times, while the ensemble average, that is the statistical average across all topological sectors, vanishes like $1/t$. One is tempted to conclude that the vacuum is a dilute gas of instantons. However, this is not the case. We find a negative value for the 'kurtosis', $K = \langle Q^4\rangle_c/\langle Q^2\rangle_c$, on all lattice volumes, while $K = 1$ for a dilute instanton gas. Unlike cooling, the gradient flow keeps the topological sectors disconnected far beyond $\sqrt{8t} = L$.

If our general expectation is correct and the color charge is screened for $|\theta| > 0$, we should, in the first place, find that the coupling constant vanishes for nonvanishing values of θ. From $\langle E(Q,t)\rangle$ we obtain the running coupling $\alpha_V(Q,\mu)$ depending of Q. In Fig. 5 we show $\alpha_V(Q,\mu)$

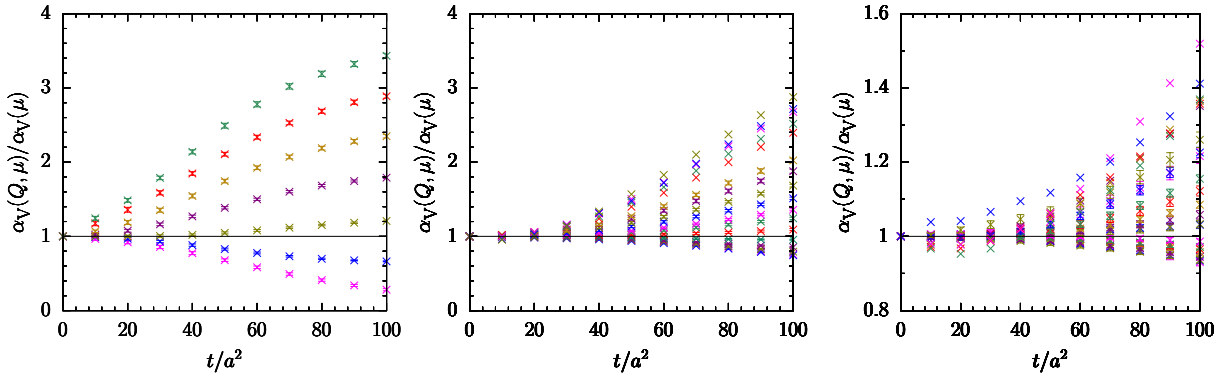

Figure 5: The ratio $\alpha_V(Q,\mu)/\alpha_V(\mu)$ as a function of t/a^2 on the 16^4 (left), 24^4 (center) and 32^4 (right) lattice for charges ranging from $Q = 0$ (bottom) to $|Q| = 6$, 16 and 22 (top), respectively. On the 24^4 and 32^4 lattices no errorbars are shown for extreme values of Q because of limited statistics.

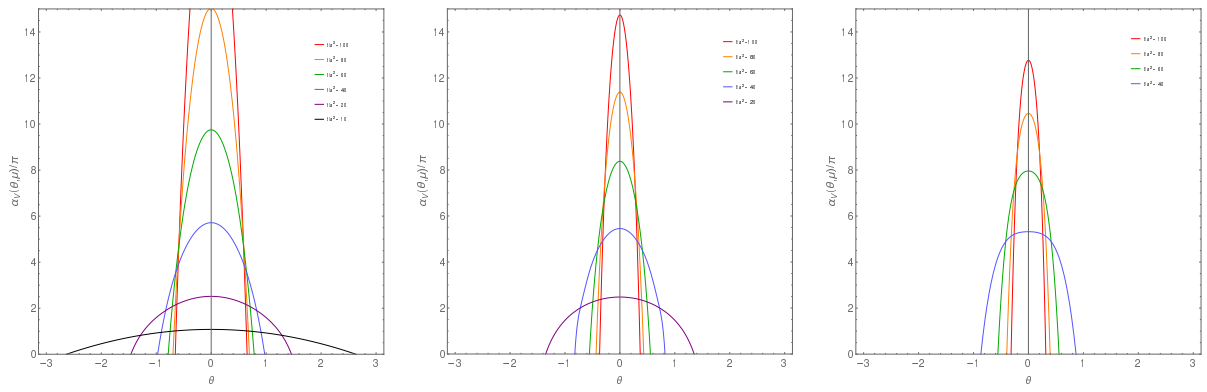

Figure 6: The running coupling $\alpha_V(\theta,\mu)$ as a function of θ on the 16^4 (left), the 24^4 (center) and the 32^4 (right) lattice for flow times from $t/a^2 = 10$, 20 and 40 to 100, respectively.

divided by the ensemble average $\alpha_V(\mu)$ as a function of t/a^2 and Q. On the 24^4 and 32^4 lattices our ensemble consists of only a few configurations at higher values of Q, hence the seemingly large fluctuation. Already at relatively small flow times $\alpha_V(Q,\mu)$ fans out according to Q. The smaller separations on larger volumes are balanced by the weight of the functional integrand. Interestingly, $\alpha_V(Q,\mu)$ vanishes in the infrared for $Q = 0$, while the ensemble average $\alpha_V(\mu)$, shown by the solid line, is represented by $|Q| \simeq \sqrt{2\langle Q^2\rangle/\pi}$. The transformation of $\alpha_V(Q,\mu)$ to the θ vacuum is achieved by the Fourier transform

$$\alpha_V(\theta,\mu) = \frac{1}{Z(\theta)} \sum_Q e^{i\theta Q} P(Q)\, \alpha_V(Q,\mu)\,, \quad Z(\theta) = \sum_Q e^{i\theta Q} P(Q)\,, \tag{17}$$

where $P(Q)$ is the probability distribution of the topological charge Q with $\sum_Q P(Q) = 1$. To compensate for the fluctuations of $P(Q)$ and $\alpha_V(Q,\mu)$ at extreme values of Q, we flattened the tail of the distributions by fitting it to an appropriate function. The result is presented in Fig. 6 for our three volumes. It clearly shows that the color charge is totally screened for $|\theta| \gtrsim 0$ in the infrared, that is at long distances, while $\alpha_V(\theta,\mu)$ becomes gradually independent of θ as we approach the perturbative, short-distance regime. With increasing flow time $\alpha_V(\theta,\mu)$ becomes an increasingly narrow function of θ. Assuming a Gaussian distribution for $P(Q)$ and using $V\langle E(Q,t)\rangle/8\pi^2 \simeq |Q|$ we derive $\alpha_V(\theta,\mu)/\alpha_V(\mu) \simeq 1 - 0.13\,(t/a^2)\,\theta^2$ on the 32^4 lattice for large flow times and small values of θ, which roughly describes the effect.

With our current statistics we are not able to compute $\alpha_V(\theta,\mu)$ with confidence for $t/a^2 \lesssim 20$ and 40 on the 24^4 and 32^4 lattice, respectively. But there is no doubt that it will continue to flatten off as seen on the 16^4 lattice. The reason is twofold. Both numerator and denominator in eq. (17) drop sharply with θ on large volumes, and one quickly runs into a zero-over-zero limit at larger values of θ. A further hindrance is that fluctuations of $\alpha_V(Q,\mu)$ with Q can be severe on large volumes before the ensemble has settled into truly disconnected topological sectors, as can be seen in Fig. 6. The situation is expected to improve for smaller lattice spacings a.

The Polyakov loop, which represents a single static quark travelling around the periodic lattice, should be screened for $|\theta| > 0$ as well. We show the bare Polyakov loop correlator $\langle|P|^2\rangle_Q$, depending on Q, as a function of t/a^2 in Fig. 7. Also shown is a scatter plot of P at

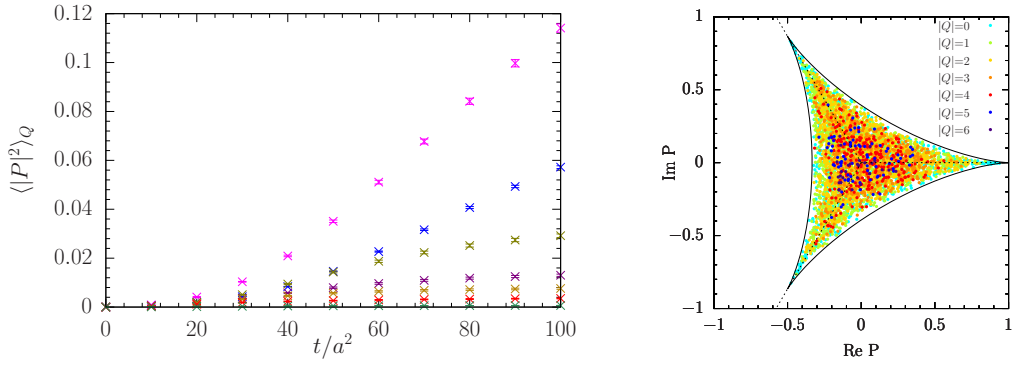

Figure 7: Left panel: The Polyakov loop correlator $\langle|P|^2\rangle_Q$ as a function of t/a^2 for $|Q| = 0$ (top) to $|Q| = 6$ (bottom). Right panel: The Polyakov loop P for $t/a^2 = 60$ according to charge $|Q|$. Both plots are on the 16^4 lattice.

$t/a^2 = 60$. Both plots are on the 16^4 lattice, where we have the highest count per charge. We find $\langle P\rangle = 0$ in each sector. That implies center symmetry for all values of θ. The figure on the right shows that for small values of $|Q|$ the Polyakov loop P rapidly populates the entire theoretically allowed region while it stays small for larger values of $|Q|$. Similar results are found on the larger lattices. In the θ vacuum we have

$$\langle|P|^2\rangle_\theta = \frac{1}{Z(\theta)}\sum_Q e^{i\theta Q}\,P(Q)\,\langle|P|^2\rangle_Q\,, \quad \langle|P|\rangle_\theta = \frac{1}{Z(\theta)}\sum_Q e^{i\theta Q}\,P(Q)\,\langle|P|\rangle_Q\,, \tag{18}$$

from which we derive the (re)normalized Polyakov loop susceptibility

$$\chi_P(\theta) = \frac{\langle|P|^2\rangle_\theta - \langle|P|\rangle_\theta^2}{\langle|P|\rangle_\theta^2}\,, \tag{19}$$

which describes the color-line connected part of the Polyakov loop correlator $\langle|P|^2\rangle_\theta$. We show

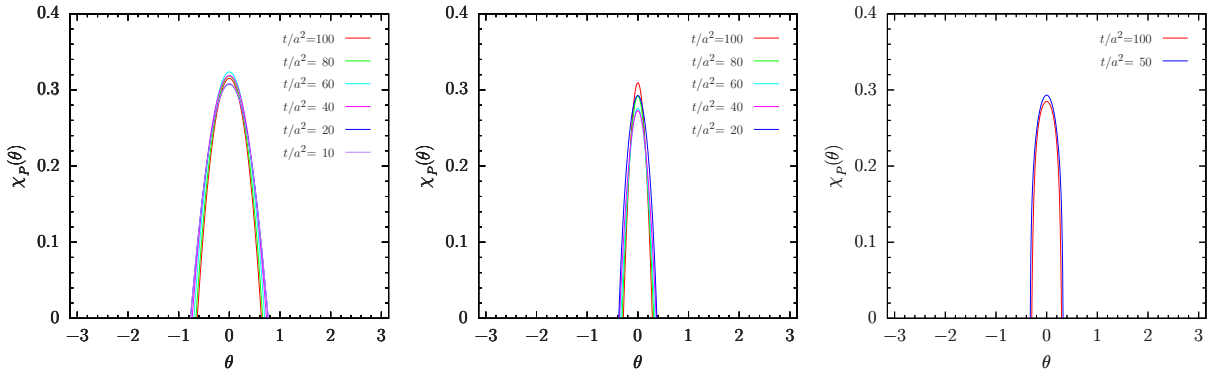

Figure 8: The Polyakov susceptibility $\chi_P(\theta)$ as a function of θ on the 16^4 (left), 24^4 (center) and 32^4 (right) lattice for flow times from $t/a^2 = 10$, 20 and 50 to 100, respectively. The peak values have been shown in Fig. 2 already.

the Polyakov loop susceptibility $\chi_P(\theta)$ in Fig. 8 for $t/a^2 = 10$ to 100. Other than the color charge, the Polyakov loop gets totally screened for $|\theta| \gtrsim 0$ already at $\sqrt{t} \approx 0.25\,\text{fm}$ (and perhaps way below), thus assuming the free field value $\chi_P = 0$. Furthermore, the Polyakov loop susceptibility turns out to be independent of the flow time, which indicates that it has been properly renormalized for all values of θ. Some finite volume effects are seen on the 16^4 lattice. The Polyakov loop is somewhat special, as it can readily be screened by static dyon loops wrapped around the lattice [9, 28]. Similar plots, largely identical in shape, are obtained for the (normalized) susceptibility $\chi_Q(\theta)$, with P substituted by Q in eq. (19) and $\chi_Q(0) \approx 1.75\chi_P(0)$. (See the text after eq. (9).) This means the topological charge gets screened for $|\theta| \gtrsim 0$ as well. Again, we cannot compute $\chi_P(\theta)$ for smaller values of t/a^2 on the larger lattices at present for reasons given above.

For the sake of clarity we have not shown error envelopes in Figs. 6 and 8. In Fig. 6 the vertical error is estimated at 2%, but no smaller than 0.2, and the horizontal error is about 10%. In Fig. 8 the vertical error is estimated at 6%, but no smaller than 0.02, and the horizontal error is about 15%.

We may extend the calculation of the static potential in eq. (16) to nonvanishing values of θ. In this case the θ parameter acts as an infrared cut-off on $\alpha_V(\theta, q)$, which results in $\sigma = 0$ for all values $|\theta| > 0$, in accord with the Polyakov loop susceptibility.

5 Conclusions

The gradient flow proved a powerful tool for tracing the evolution of the gauge field over successive length scales for any initial coupling. It passed several tests and showed its potential for extracting low-energy quantities of the theory. The novel result is that color charges are screened for $|\theta| > 0$ in the nonperturbative regime, limiting the vacuum angle to $\theta = 0$ at long distances, which rules out any strong CP violation at the hadronic level.

Not much changes in three-flavor QCD for heavy quarks. In Fig. 9 we plot $\alpha_{GF}(\mu)$ as a

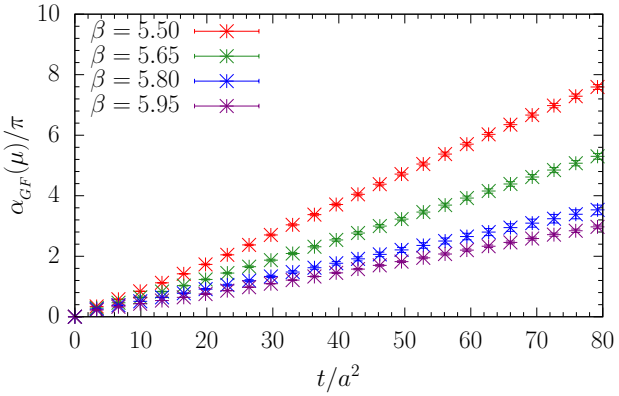

Figure 9: The gradient flow coupling $\alpha_{GF}(\mu)/\pi$ for QCD with three flavors of dynamical quarks at the SU(3) flavor symmetric point for $\beta = 5.50$, 5.65, 5.80 and 5.95 on the $32^3 \times 64$ ($\beta = 5.50$ and 5.65) and the $48^3 \times 96$ ($\beta = 5.80$ and 5.95) lattice. The lattice spacings range from $a = 0.074\,\text{fm}$ at $\beta = 5.50$ to $a = 0.051\,\text{fm}$ at $\beta = 5.95$ [18].

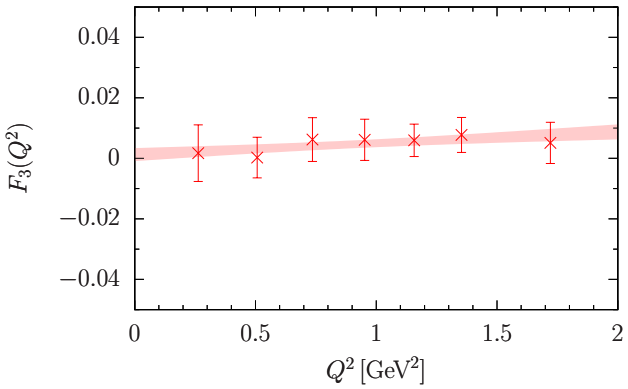

Figure 10: The dipole form factor $F_3(Q^2)$ of the neutron on the $32^3 \times 64$ lattice at the SU(3) flavor symmetric point $m_\pi = m_K = 410\,\mathrm{MeV}$ [18] for $|\theta| \approx 0.4$ and $\beta = 5.50$.

function of t/a^2 at the SU(3) flavor symmetric point [27], $m_\pi = m_K = 410\,\mathrm{MeV}$, for four different values of β. The individual curves fall onto a single straight line when transformed to a common scale. As before, the gauge fields split into disconnected topological sectors at large flow times. A flavor-diagonal CP-violating phase of the quark mass matrix, which can be traced back to closed loops of chiral zero modes [29], can be rotated into a θ term in accord with the Atiyah-Singer index theorem. Hence, the mechanism that screens the color charge in the Yang-Mills theory can be expected to screen the color fields in QCD too.

Lattice calculations of CP violating observables, like the electric dipole moment of the nucleon and the $\eta^{(\prime)} \to \pi\pi$ decay amplitude, are necessarily done at large cut-off scales $\mu \propto 1/a$. In the absence of a phase transition, we should find any physical quantity evaluated at (μ, θ) to be connected with its value at $(\mu, \theta) \rightsquigarrow (0, 0)$ by a RG trajectory. Consequently, the dipole moment, for example, should vanish for any value of (μ, θ).

An attempt of deriving 'RG equations' for the running coupling $\alpha_V(\theta, \mu)$ has been made in [20, 30], by analogy with the quantum Hall conductivity [31]. Qualitatively, $\partial\theta/\partial \ln t \propto -\theta$ for small θ and large t. That is, θ is driven to zero at long distances. We expect the theory to have a rich phase structure however and the relevant degrees of freedom, which permit a simple formulation of the low-energy properties, to be different from the microscopic ones and have their own critical behavior.

The dipole moment mentioned provides a crucial test of our results. If it exists, it should be largest for massive quarks. In [32] we have computed $d_n = eF_3(0)/2m_N$ from a fully dynamical simulation of $2+1$ flavors of clover fermions including the θ term. The calculation follows [33], corrected for spurious mixing effects with the Pauli form factor F_2 [34]. Fig. 10 shows the dipole form factor F_3 of the neutron at the SU(3) flavor symmetric point for $|\theta| \approx 0.4$. This leads to $d_n = 0.00028(30)\,[\mathrm{e\,fm}\,\theta]$, which is compatible with zero, as expected. Similar results have been reported in [34, 35].

The nontrivial phase structure of QCD greatly affects anomalous chiral transformations. Whatever the new phases are - Higgs, Coulomb or oblique confinement -, our results leave no room for axions. The QCD vacuum will be unstable under the Peccei-Quinn chiral $U_{PQ}(1)$ transformation [36], realized by the shift symmetry $\theta \to \theta + \delta$, which thwarts the axion conjecture.

Acknowledgment

The numerical computations have been carried out on the HOKUSAI at RIKEN and the Xeon cluster at RIKEN R-CCS using BQCD [37, 38].

References

[1] C. Abel *et al.*, Phys. Rev. Lett. **124** (2020) 081803 [arXiv:2001.11966 [hep-ex]].

[2] S. R. Coleman, Annals Phys. **101** (1976) 239.

[3] C. G. Callan, R. F. Dashen and D. J. Gross, Phys. Rev. D **20** (1979) 3279.

[4] G. 't Hooft, Nucl. Phys. B **190** (1981) 455.

[5] A. S. Kronfeld, G. Schierholz and U. J. Wiese, Nucl. Phys. B **293** (1987) 461.

[6] A. S. Kronfeld, M. L. Laursen, G. Schierholz and U. J. Wiese, Phys. Lett. B **198** (1987) 516.

[7] E. Witten, Phys. Lett. B **86** (1979) 283.

[8] J. L. Cardy and E. Rabinovici, Nucl. Phys. B **205** (1982) 1.

[9] V. Bornyakov and G. Schierholz, Phys. Lett. B **384** (1996) 190 [arXiv:hep-lat/9605019 [hep-lat]].

[10] R. Narayanan and H. Neuberger, JHEP **0603** (2006) 064 [hep-th/0601210].

[11] M. Lüscher, JHEP **1008** (2010) 071, Erratum: JHEP **1403** (2014) 092 [arXiv:1006.4518 [hep-lat]].

[12] M. Lüscher, PoS LATTICE **2013** (2014) 016 [arXiv:1308.5598 [hep-lat]].

[13] H. Makino, O. Morikawa and H. Suzuki, PTEP **2018** (2018) 053B02 [arXiv:1802.07897 [hep-th]].

[14] Y. Abe and M. Fukuma, PTEP **2018** (2018) 083B02 [arXiv:1805.12094 [hep-th]].

[15] A. Carosso, A. Hasenfratz and E. T. Neil, Phys. Rev. Lett. **121** (2018) 201601 [arXiv:1806.01385 [hep-lat]].

[16] M. Lüscher and P. Weisz, JHEP **02** (2011) 051 [arXiv:1101.0963 [hep-th]].

[17] K. G. Wilson, Phys. Rev. D **10** (1974) 2445.

[18] V. G. Bornyakov, R. Horsley, R. Hudspith, Y. Nakamura, H. Perlt, D. Pleiter, P. E. L. Rakow, G. Schierholz, A. Schiller, H. Stüben and J. M. Zanotti, [arXiv:1508.05916 [hep-lat]].

[19] N. Miller, L. C. Carpenter, E. Berkowitz, C. C. Chang, B. Hörz, D. Howarth, H. Monge-Camacho, E. Rinaldi, D. A. Brantley and C. Körber, C. Bouchard, M. A. Clark, A. S. Gambhir, C. J. Monahan, A. Nicholson, P. Vranas and A. Walker-Loud, Phys. Rev. D **103** (2021) 054511 [arXiv:2011.12166 [hep-lat]].

[20] Y. Nakamura and G. Schierholz, PoS LATTICE **2019** (2019) 172 [arXiv:1912.03941 [hep-lat]].

[21] M. Cè, C. Consonni, G. P. Engel and L. Giusti, Phys. Rev. D **92** (2015) 074502 [arXiv:1506.06052 [hep-lat]].

[22] Y. Schröder, Phys. Lett. B **447** (1999) 321 [arXiv:hep-ph/9812205 [hep-ph]].

[23] M. Dalla Brida and A. Ramos, Eur. Phys. J. C **79** (2019) 720 [arXiv:1905.05147 [hep-lat]].

[24] J. L. Richardson, Phys. Lett. B **82** (1979) 272.

[25] E.-M. Ilgenfritz, M.L. Laursen, G. Schierholz, M. Müller-Preussker and H. Schiller, Nucl. Phys. B **268** (1986) 693.

[26] C. Bonati and M. D'Elia, Phys. Rev. D **89** (2014) 105005 [arXiv:1401.2441 [hep-lat]].

[27] W. Bietenholz, V. Bornyakov, M. Göckeler, R. Horsley, W. G. Lockhart, Y. Nakamura, H. Perlt, D. Pleiter, P. E. L. Rakow, G. Schierholz, A. Schiller, T. Streuer, H. Stüben, F. Winter and J. M. Zanotti, Phys. Rev. D **84** (2011) 054509 [arXiv:1102.5300 [hep-lat]].

[28] M. L. Laursen and G. Schierholz, Z. Phys. C **38** (1988) 501.

[29] D. Guadagnoli, V. Lubicz, G. Martinelli and S. Simula, JHEP **04** (2003) 019 [arXiv:hep-lat/0210044 [hep-lat]].

[30] V. G. Knizhnik and A.Y. Morozov, JETP Lett. **39** (1984) 240 [Pisma Zh. Eksp. Teor. Fiz. **39** (1984) 202].

[31] H. Levine, S. B. Libby and A. M. M. Pruisken, Phys. Rev. Lett. **51** (1983), 1915 [erratum: Phys. Rev. Lett. **52** (1984) 1254]; H. Levine and S. B. Libby, Phys. Lett. B **150** (1985) 182.

[32] M. Batelaan, F.-K. Guo, U.-G. Meißner, Y. Nakamura, G. Schierholz, J. M. Zanotti *et al.*, "The electric dipole moment of the neutron from 2+1 flavor lattice QCD: an update", in preparation.

[33] F.-K. Guo, R. Horsley, U.-G. Meißner, Y. Nakamura, H. Perlt, P.E.L. Rakow, G. Schierholz, A. Schiller and J.M. Zanotti, Phys. Rev. Lett. **115** (2015) 062001 [arXiv:1502.02295 [hep-lat]].

[34] M. Abramczyk, S. Aoki, T. Blum, T. Izubuchi, H. Ohki and S. Syritsyn, Phys. Rev. D **96** (2017) 014501 [arXiv:1701.07792 [hep-lat]].

[35] C. Alexandrou, A. Athenodorou, K. Hadjiyiannakou and A. Todaro, Phys. Rev. D **103** (2021) 054501 [arXiv:2011.01084 [hep-lat]].

[36] R. D. Peccei and H.R. Quinn, Phys. Rev. Lett. **38** (1977) 1440; Phys. Rev. D **16** (1977) 1791.

[37] Y. Nakamura and H. Stüben, PoS **LATTICE2010** (2010) 040 [arXiv:1011.0199 [hep-lat]].

[38] T. R. Haar, Y. Nakamura and H. Stüben, EPJ Web Conf. **175** (2018) 14011 [arXiv:1711.03836 [hep-lat]].